ORIGINAL PAPER

T. T. Mai · J. W. Schultze · G. Staikov

Relation between surface preconditioning and metal deposition in direct galvanic metallization of insulating surfaces

Abstract The relation between surface preconditioning and metal deposition in the direct galvanic metallization of different insulating polymer surfaces by the so-called PLATO technique was studied using electrochemical and surface analytical methods. AFM, XPS and contact angle measurements show that the chromic acid etching of original polymer surfaces leads to an increase of the surface energy and hydrophilicity of polymer substrates due to both surface roughening and the formation of -COOH and/or -COH surface groups. However, decisive for the subsequent surface activation with cobalt sulfide is the increase in surface roughness. The influence of the degree of activation and the electrode potential on the kinetics of Ni metallization was studied by current transient measurements on activated line-shaped structures. The results suggest that the electrochemical reduction of cobalt sulfide to cobalt is a necessary step to induce the process of Ni electrodeposition. Successful Ni metallization could be obtained on ABS (acrylonitrile-butadiene-styrene) and PEEK (poly-ether-ether-ketone) surfaces. The lateral propagation rate, V_x, of the depositing Ni layer depends exponentially on the applied potential and was found to be several orders of magnitude higher than the Ni deposition rate, V_z, in the normal z-direction ($V_x/V_z = 10^2$–10^4). It was demonstrated that the approach involving cobalt sulfide pre-activation can also be applied successfully for metallization of oxidized porous silicon surfaces.

T. T. Mai · J. W. Schultze · G. Staikov (✉)
Institut für Physikalische Chemie und Elektrochemie,
Heinrich-Heine Universität Düsseldorf,
40225 Dusseldorf, Germany
E-mail: georgi.staikov@uni-duesseldorf.de
Tel.: +49-211-8113686
Fax: +49-211-8112803

Introduction

Metallization of insulating polymers is of great importance for numerous applications in the electronics and car industries. The most frequently used processes for metallization are physical vapor deposition (PVD), chemical vapor deposition (CVD) and electroless metal deposition [1]. Nevertheless, a lot of effort has been made to obtain a method to metallize modified insulating substrates by direct metal electrodeposition (direct galvanic metallization) [2, 3, 4, 5, 6, 7, 8, 9]. The process of direct electrodeposition offers a number of advantages, including simple control of metallization by current density and electrode potential, achievement of high deposition rates at relatively low operating temperatures, high selectivity and possibilities for metallization of surfaces and microstructures with complicated surface profiles. An original method for direct metallization of insulating polymer surfaces called the PLATO technique has been proposed recently by Möbius et al. [7, 8, 9]. The key step of this method is the activation of the polymer surface with an appropriate metal sulfide. The electrodeposition process is induced by applying a point contact to the metal sulfide seed layer. The resulting metallization is characterized by a fast lateral propagation of the depositing metal layer, a behaviour that is very attractive for various applications in microelectronics and microsystem technology. This characteristic metallization behaviour, however, is still not understood and requires detailed studies on the role of the nature and the preconditioning (etching and activation) of the polymer surfaces in the overall metallization process.

In this paper we report studies on the relation between surface preconditioning and Ni electrodeposition in the direct galvanic metallization of different insulating surfaces using cobalt sulfide as an activator.

Experimental

The polymer substrates used in this study were acrylonitrile-buta-diene-styrene (ABS), poly-ether-ether-ketone (PEEK) and polyi-mide (PI), all supplied by Good Fellows, USA. The chemical and phase compositions of these materials are given in Table 1.

The preconditioning and metallization of all polymer substrates were performed in the same way according to the PLATO technique [7, 8, 9]. The first step was a wet chemical etching in a chromic acid solution (CrO_3/H_2SO_4) at 65 °C for 5 min to increase the roughness and hydrophilicity of the polymer surfaces. After this pre-treatment the surfaces were activated with cobalt sulfide. The activation is based on the so-called adsorption concept and includes the following two steps: (1) dipping the polymer substrates into a commercial solution containing cobalt(II) sulfate, ammonia and an oxidizer (Enthone, Germany) at room temperature for 2 min and (2) subsequent sulfidization in Na_2S solution for 1 min. After each step the samples were thoroughly cleaned in Millipore water. The metallization of the polymer surfaces was performed at 45 °C by electrodeposition of Ni under potentiostatic conditions from a Watts electrolyte bath (150 g/L $NiSO_4.6H_2O$, 30 g/L $NiCl_2.6H_2O$, 30 g/L H_3BO_3, pH 4) in a conventional three-electrode electrochemical cell with a Hg/Hg_2SO_4/1 M Na_2SO_4 reference electrode and a Ni-plate counter electrode. All electrode potentials are referred to the potential of the standard hydrogen electrode (SHE). A Pt tip was used to contact the activated polymer surface and to induce electrodeposition. The contact area of the Pt tip was reduced by appropriate insulation with Apiezon wax. The lateral propagation of the Ni layer was investigated by current transient measurements and microscopic observations. Current transient measurements were performed on line-shaped structures (0.8 mm×12 mm) prepared by selective activation, applying a mask on the etched polymer surface. Additional cyclic voltammetric measurements in Ni^{2+}-free and Ni^{2+}-containing electrolytes were performed on glassy carbon (GC) substrates in order to obtain information on the electrochemical behaviour of cobalt sulfide.

The topography and roughness of the polymer surfaces were characterized by atomic force microscopy (AFM) using commercial equipment (PicoSPM, Molecular Imaging, and Nanoscope E Controller, Digital Instruments, USA). The surface composition and the chemical states were investigated by X-ray photoelectron spectroscopy (XPS) using a modified ESCALAB-V (VG Instruments, UK). XPS measurements were carried out at a base pressure of 10^{-10} mbar with polychromatic Al K_α radiation (1486.6 eV),

CAE mode, a pass energy of 50 eV for survey scans and 20 eV for specific element scans. Ion etching was performed by an AG-S2 ion source with argon pressure of 1.5×10^{-5} mbar and an acceleration potential of 4 kV. A computer program for peak deconvolution (Unifit v.2.4, University of Leipzig, Germany) was used to analyse quantitatively the XPS peaks.

Contact angle measurements were performed at room temperature (23–25 °C) in a glass chamber using the so-called sessile drop technique with Millipore water as a liquid. Water drops (with a diameter of about 2 mm) were introduced onto the substrate surface through a microsyringe, taking special care to avoid vibrations of the system. The time for achieving equilibrium was 3 min.

Results and discussion

Etching of polymer surfaces

Information on the surface topography of the etched and original (untreated) polymer materials was obtained by AFM. Figure 1 shows typical AFM images for ABS (Fig. 1a, 1a′) and PI (Fig. 1b, 1b′) substrates as an example. As seen, the chemical etching leads to the formation of pits of micrometer size on the ABS surface, whereas the surface topography of PI changes insignificantly. The root mean square (r.m.s.) roughness, R_{rms}, of treated and untreated polymer surfaces was estimated by a statistical analysis of corresponding AFM images. The obtained R_{rms} values for various substrates are summarized in Table 2.

In the case of ABS, the surface roughness increases from 30.9 nm before etching to 115.8 nm after etching. This behaviour can be explained by the much higher dissolution rate of polybutadiene in the chromic acid solution, leading to a selective etching of the polybutadiene surface domains of ABS [10, 11]. A similar etching behaviour is shown also by the PEEK substrate. In this case the observed R_{rms} increase can be attributed to an enhanced selective etching of PEEK surface domains

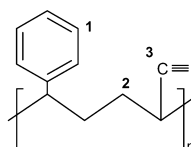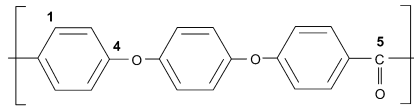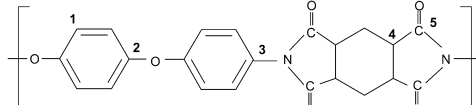**Table 1** Chemical and phase compositions of the polymer materials

polymer	chemical composition		phase composition
ABS	Styrole Acrylnitrile (SAN)	Polybutadiene (PB)	two phases (SAN and PB)
PEEK			Semi-crystalline phase
PI			amorphous phase

Fig. 1 AFM images of ABS and PI surfaces: (**a**, **b**) before and (**a′**, **b′**) after etching
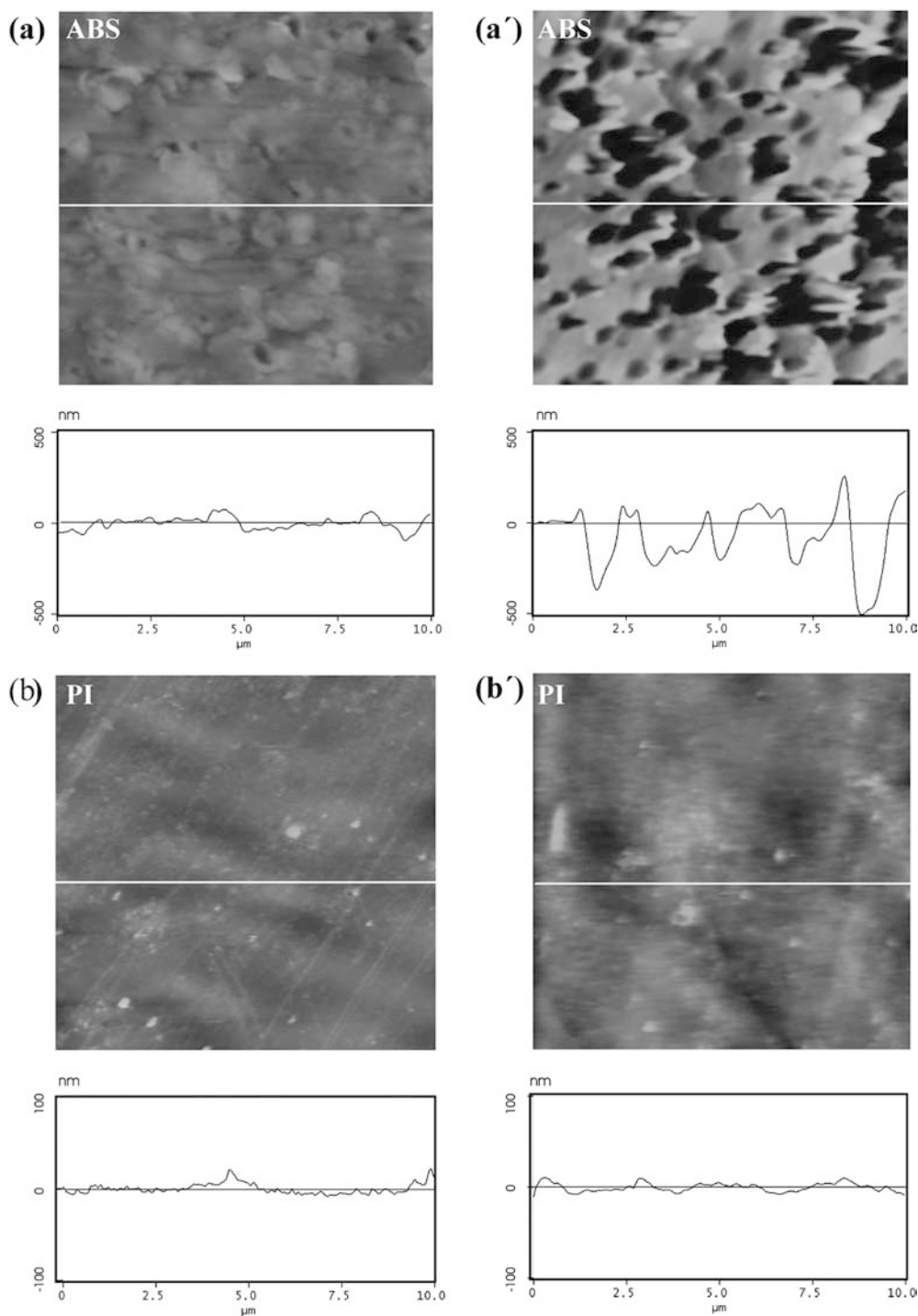

Table 2 Surface roughness, R_{rms}, and roughness factor, r, for different polymer surfaces before (o) and after (e) etching

Polymer	Original surfaces		Etched surfaces		
	R_{rms} (nm)	$r^{(o)}$	R_{rms} (nm)	$r^{(e)}$	$r^{(e)}/r^{(o)}$
ABS	30.9	1.03	115.8	1.76	1.71
PEEK	21.3	1.04	67.9	1.4	1.34
PI	7.0	1.01	10.7	1.06	1.05

with lower crystallinity [10, 12]. In contrast to ABS and PEEK, after treatment in the chromic acid solution the one-phase polymer PI shows a negligible roughness change, indicating a homogeneous etching of the surface.

The C 1s XPS spectra for different polymer surfaces before and after etching are shown in Fig. 2. The numbered deconvoluted peaks correspond to the different carbon states labelled in Table 1. The deconvolution analysis of C 1s spectra for all polymer surfaces after

Fig. 2 C 1s XP spectra: (**a**, **b**, **c**) original and (**a′**, **b′**, **c′**) etched polymer surfaces
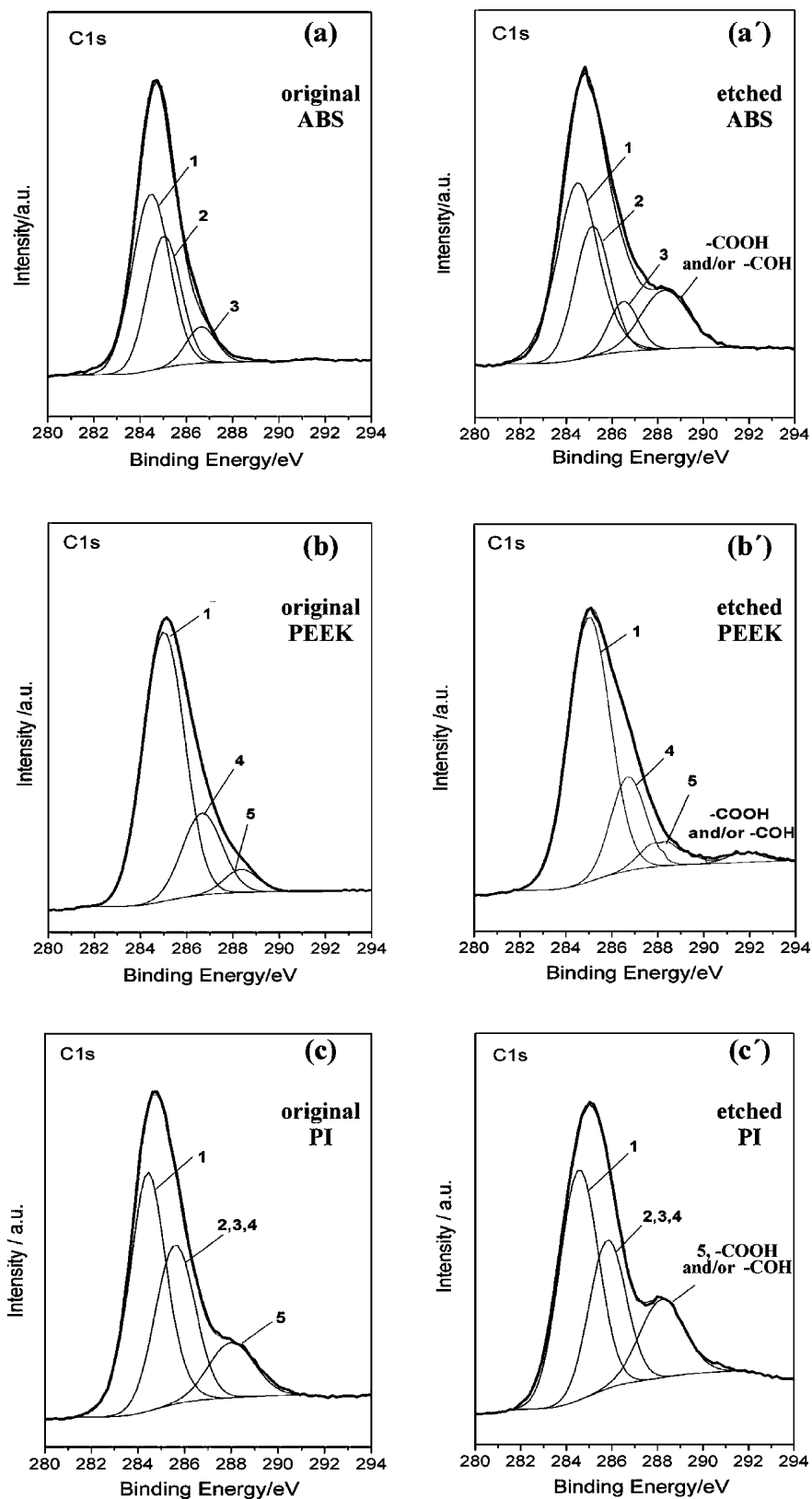
etching (cf. Fig. 2a′, 2b′ and 2c′) shows the appearance of new additional peaks at higher binding energies (288.2 and 292.2 eV). These results suggest the formation of new functional surface groups such as –COOH and/or –COH due the strong oxidation of the polymer surfaces during the etching treatment.

The change of surface energy, $\Delta\gamma$, due to the etching can be described by:

$$\Delta\gamma = \gamma^{(e)} - \gamma^{(o)} = \Delta\gamma_r + \Delta\gamma_{COOH} \qquad (1)$$

where $\Delta\gamma_r$ and $\Delta\gamma_{COOH}$ represent the contributions due to the increase of surface roughness and the formation of new –COOH and/or –COH groups, respectively. The surface energies $\gamma^{(e)}$ and $\gamma^{(o)}$ of etched (e) and original (o) polymer surfaces were determined by contact angle measurements using the modified Young–Dupre equation [13, 14]:

$$\gamma = \gamma_{\frac{w}{4}}(1 + \cos\alpha)^2 \qquad (2)$$

where $\gamma_w = 73$ mJ/m^2 is the surface energy of the liquid water and α is the measured contact angle. The measured contact angles of the original and etched surfaces, $\alpha^{(o)}$ and $\alpha^{(e)}$, as well as the values for $\gamma^{(e)}$, $\gamma^{(o)}$ and $\Delta\gamma$, are summarized in Table 3. The roughness contributions, $\Delta\gamma_r$, were estimated from the equation:

$$\Delta\gamma_r = \frac{\gamma_w}{4}\left[\left(1 + \cos\alpha_r^{(e)}\right)^2 - \left(1 + \cos\alpha^{(o)}\right)^2\right] \qquad (3)$$

In this equation, $\alpha_r^{(e)}$ represents the expected contact angle of the etched surface by considering only the effect of roughness increase. The $\alpha_r^{(e)}$ values were calculated from the roughness factors $r^{(e)}$ and $r^{(o)}$ of the original and etched polymer surfaces determined by AFM (cf. Table 2) using the Wenzel relation [15]:

$$\cos\alpha_r^{(e)} = \frac{r^{(e)}}{r^{(o)}}\cos\alpha^{(o)} \qquad (4)$$

The estimated $\Delta\gamma_r$ and $\Delta\gamma_{COOH}$ contributions to $\Delta\gamma$ for different polymer substrates are presented in Fig. 3. The results show that the large surface energy increase of ABS and PEEK is mainly due to the increase of the surface roughness during the etching treatment, whereas the surface energy of PI increases predominantly due to the formation of –COOH (and/or –COH) surface groups.

Surface activation

Figure 4 shows typical XP survey spectra of etched polymer surfaces after activation with cobalt sulfide. All spectra contain not only the expected signals for Co and S, but also characteristic C and O peaks, indicating that

Table 3 Contact angles, α, and surface energies, γ, for different polymers before (o) and after (e) etching

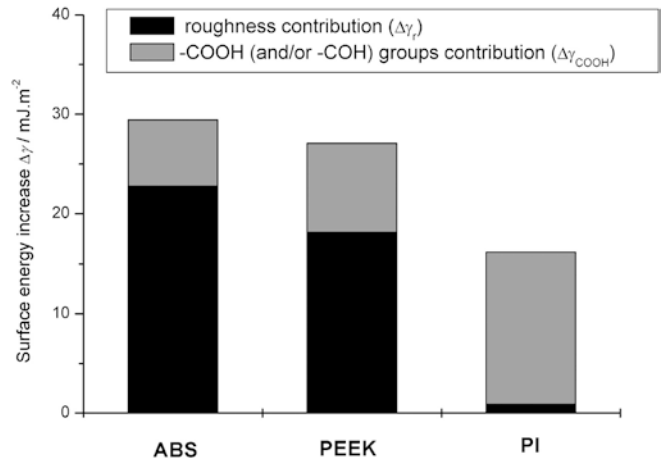| Polymer	Original surfaces		Etched surfaces		
	$\alpha^{(o)}$	$\gamma^{(o)}$ (mJ/m^2)	$\alpha^{(e)}$	$\gamma^{(e)}$ (mJ/m^2)	$\Delta\gamma = \gamma^{(e)} - \gamma^{(o)}$ (mJ/m^2)
ABS	68°	34.5	32°	62.3	28.8
PEEK	72°	31.2	39°	57.6	26.4
PI	67°	35.2	48°	50.8	15.6

Fig. 3 Contributions of the surface roughness and the formation of -COOH and/or -COH groups to the surface energy increase of the polymer substrates after etching
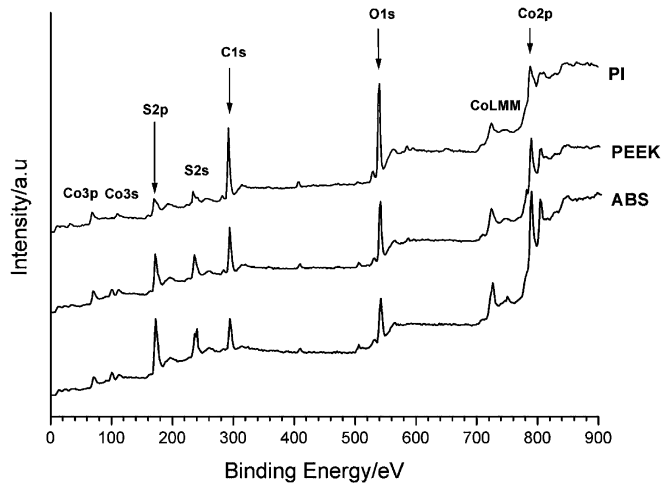

Fig. 4 XPS survey spectra of etched polymer surfaces after single activation with cobalt sulfide

the cobalt sulfide layer does not cover the polymer surface completely.

Information about the surface coverage θ of cobalt sulfide was obtained by an analysis of the XP spectra based on the equation [10]:

$$\theta = \frac{A_{Co}/S_{Co} + A_S/S_S}{\sum_i A_i/S_i} \text{ with } i = Co, S, C, O \qquad (5)$$

In this equation the ratio A_i/S_i is proportional to the surface concentration of the element i, and A_i and S_i represent the corresponding XPS peak areas and sensitivity factors, respectively. θ values of 17%, 32% and 49% were estimated from the experimental spectra in Fig. 4 for activated PI, PEEK and ABS surfaces, respectively. These results correlate well with the surface roughness data of those polymers in Table 2 and indicate that the surface topography plays an important role

in the activation process. Figure 5a shows typical XPS sputter depth profiles of Co and C for an ABS surface after single activation. As can be seen, the Co signal disappears after 120 min sputtering, corresponding to a depth of about 600 nm, which is comparable to the depth of the pits observed on etched ABS surfaces by AFM (cf. Fig. 1a). It is reasonable to suggest from these results that cobalt sulfide clusters are located preferentially in the pits of the etched ABS surface, as schematically shown in Fig. 5b. It was found that repeating the activation procedure several times increases the cobalt sulfide coverage θ of ABS and PEEK significantly. Figure 6 shows θ as a function of repeated activation cycles for ABS. As can be seen, after a single activation, θ is 49% and reaches an approximately constant value of about 86% after four activation cycles. In contrast to ABS and PEEK, no increase of θ could be detected by multiple activation of PI, which can be explained by the relatively low surface roughness of this material after etching (cf. Table 2).

Metal electrodeposition

Experimental results show that both the cobalt sulfide coverage θ and the potential E of the contact Pt tip determine the initiation of nickel electrodeposition. The electroplating process could be induced only on activated
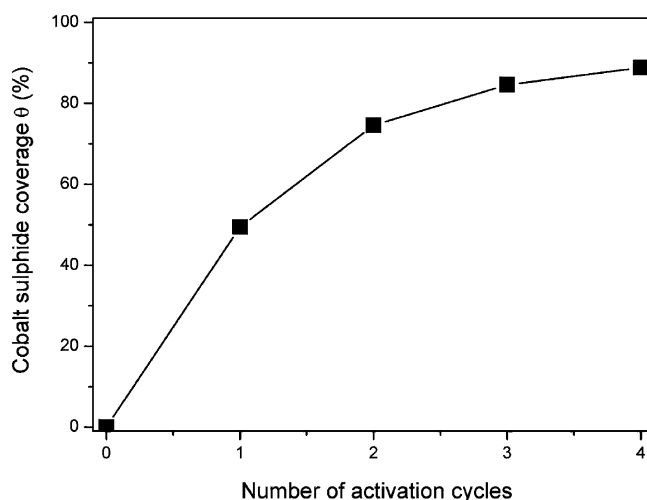
Fig. 6 Dependence of the cobalt sulfide coverage θ on the number of activation cycles for an etched ABS surface

ABS and PEEK substrates, which exhibit relatively high cobalt sulfide coverage ($\theta > 30\%$). The initiation of electrodeposition, however, was found to be possible only by application of potentials more cathodic than a critical potential located in the potential range $-0.4\ \mathrm{V} > E_{\mathrm{crit}} > -0.5\ \mathrm{V}$. Additional cyclic voltammetric measurements on cobalt sulfide modified GC substrates in Ni^{2+}-free and Ni^{2+}-containing electrolytes showed that this potential range overlaps with the potential range in which cobalt sulfide is reduced electrochemically (Fig. 7). Characteristic cathodic peaks (C_1 and C_2) observed in the cyclic voltammograms are obviously related to the electrochemical reduction of cobalt sulfide to cobalt. Cyclic voltammograms in Ni^{2+}-containing electrolytes (Fig. 7b) indicate that the formed cobalt clusters enhance nucleation processes in the initial stages of Ni electrodeposition. These results suggest that the electrochemical reduction of cobalt sulfide is a necessary step to induce the process of metallization of insulating substrates.

The kinetics of lateral propagation of the Ni layer was investigated by current transient measurements on activated line-shaped structures. The contact Pt tip was positioned at one edge of the structures, as indicated schematically in Fig. 8a. Typical current transients for metallization of activated line-shaped structures on ABS are shown in Fig. 8b.

The transients are characterized by an initial nearly linear current increase followed by establishment of a stationary current at a characteristic time τ. Simultaneous microscopic observations showed that τ corresponds exactly to the time at which the propagating Ni layer reaches the opposite edge of the line-shaped structure (cf. Fig. 8a). The lateral propagation rate V_x of the Ni layer was calculated using the relation $V_x = L/\tau$, where $L = 12$ mm is the length of the line-shaped structure. Figure 9 shows V_x as a function of potential E and cobalt sulfide coverage θ for ABS. Experimental results indicate that for a given θ the propagation rate V_x increases exponentially with E and can be described by:
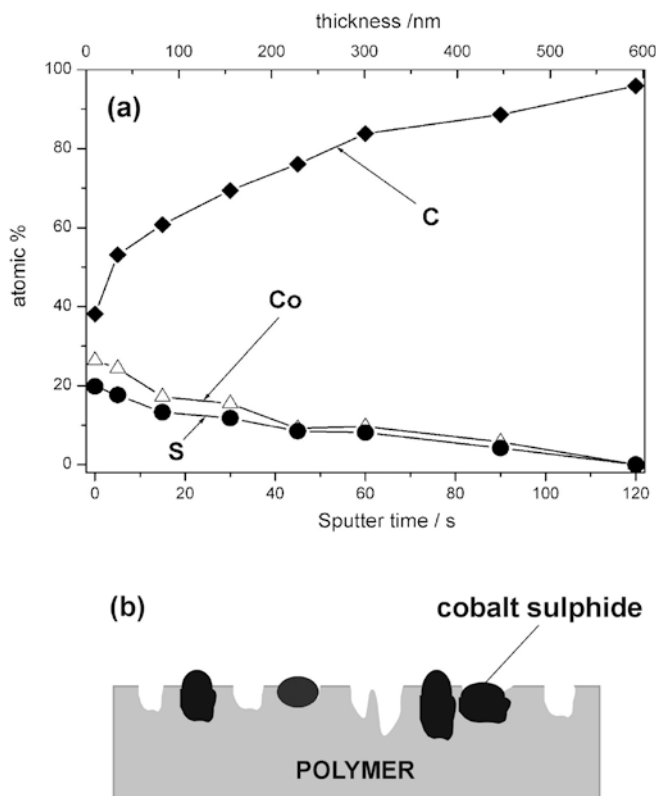

Fig. 5 (a) XPS sputter profile and (b) schematic presentation of an etched ABS surface after a single activation with cobalt sulfide (one activation cycle)
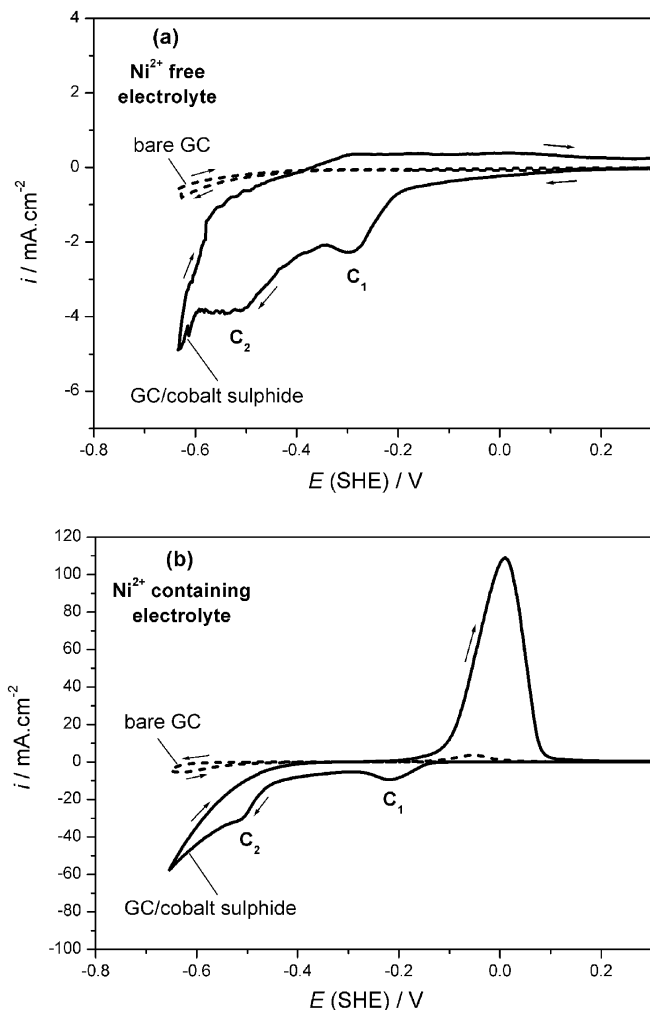
Fig. 7 Typical cyclic voltammograms of bare and cobalt sulfide modified glassy carbon (GC) substrates in (**a**) Ni^{2+}-free and (**b**) Ni^{2+}-containing electrolytes. Potential scan rate: $|dE/dt| = 1$ mV/s

Fig. 8 Lateral propagation of the Ni layer during metallization of an activated line-shaped ABS surface structure (cobalt sulfide coverage $\theta = 49\%$): (**a**) schematic representation of the experiment; (**b**) current transients at different applied potentials E

$$V_x(E)_\theta = V_x(E_{crit})_\theta \exp[k_\theta |E - E_{crit}|] \qquad (6)$$

where $V_x(E_{crit})_\theta$ represents the propagation rate at the critical potential and k_θ is a constant depending on the cobalt sulfide coverage θ. A value of $k_\theta = 0.18$ V^{-1} is obtained for single activation ($\theta = 49\%$).

The lateral propagation rate V_x is several orders of magnitude higher than the normal growth rate of the Ni layer, V_z, in the z-direction ($V_x/V_z = 10^2–10^4$). Thus, it can be suggested that Ni nucleation occurs preferentially on Co clusters formed by the electrochemical reduction of cobalt sulfide at the Ni/CoS/electrolyte three-phase boundary. Nickel layers deposited on ABS substrates using this technique have an excellent adhesion of about 1.5–2 N/mm [7]. The conductivity of these layers measured by the four-point technique was found to be within the range 1–10 S/cm for layer thicknesses varying between 0.5–1 μm.

The observed fast lateral propagation of the Ni layer makes the activation with cobalt sulfide very attractive for metallization not only of polymer substrates but also
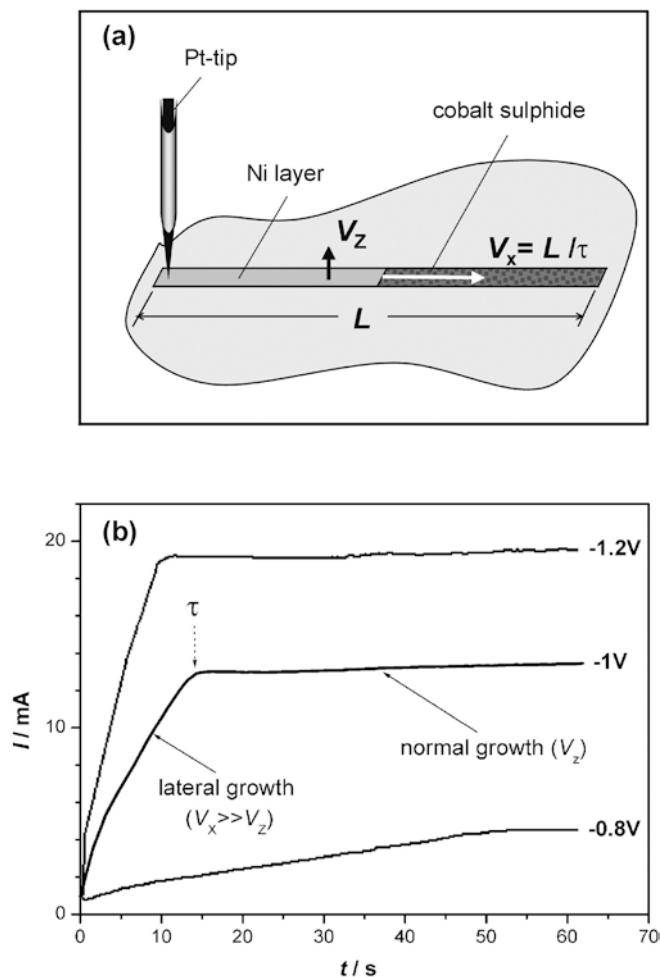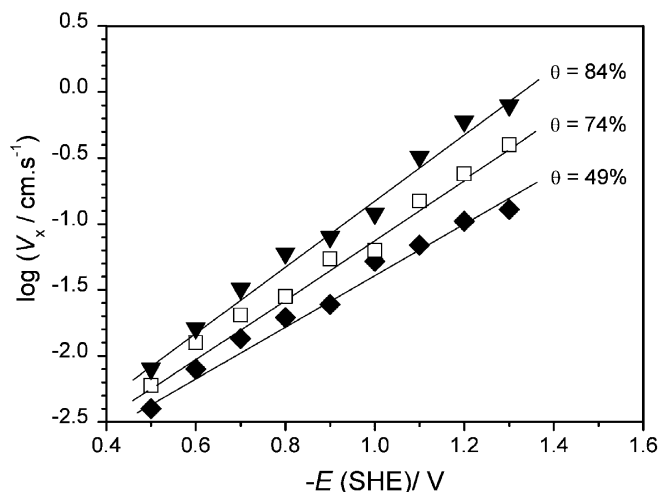

Fig. 9 Dependence of the propagation rate V_x of the Ni layer on the applied potential E and the cobalt sulfide coverage θ for metallization of ABS
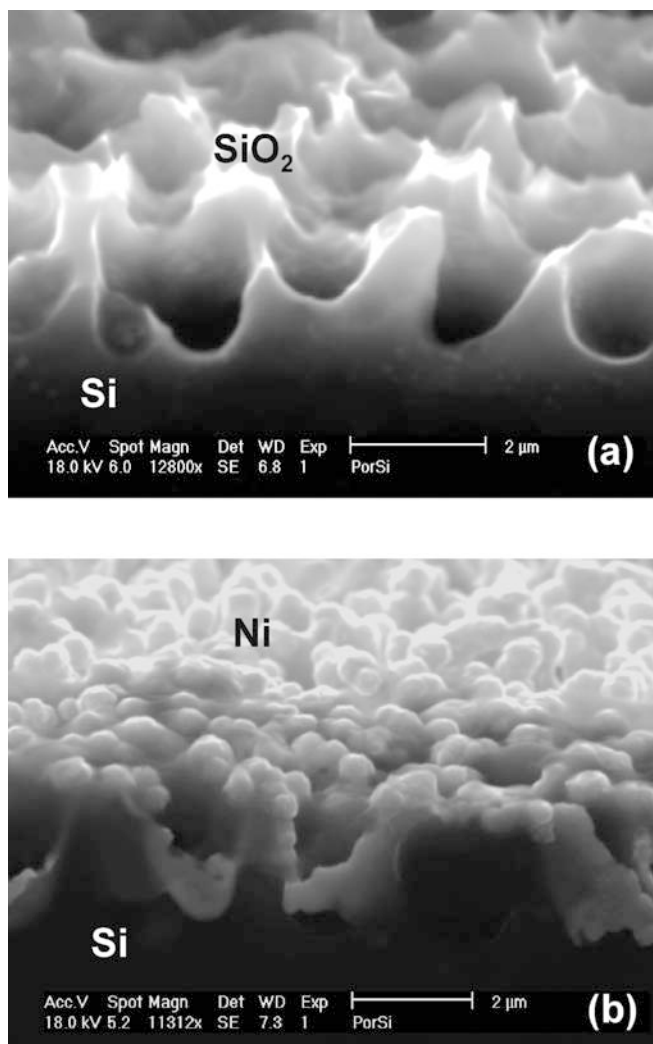
surface roughness and the formation of new functional –COOH and/or –COH surface groups. Experimental results show that crucial for subsequent activation and metallization is the increase of the surface roughness, which increases significantly the degree of activation with cobalt sulfide. Successful Ni metallization is achieved on ABS and PEEK polymer surfaces. The initiation of Ni deposition and the lateral propagation rate of the Ni layer are determined mainly by the cobalt sulfide coverage and the potential of the contacting tip. The results indicate that the electrochemical reduction of cobalt sulfide to cobalt is a necessary step to induce the process of Ni electrodeposition. The metallization of ABS and PEEK occurs by a lateral propagation of a Ni layer with a rate V_x, which is several orders of magnitude higher than the growth rate V_z in the vertical z-direction ($V_x/V_z = 10^2$–10^4). This behaviour can be successfully applied for metallization of insulating surfaces with complicated profiles and microstructures.

Fig. 10 SEM images of an oxidized porous n-Si surface: (**a**) before and (**b**) after a direct galvanic Ni metallization at a potential of $E = -0.7$ V

of oxide or ceramic surfaces exhibiting sufficient roughness. The first experimental studies in this direction were carried out on oxidized porous silicon surfaces. These surfaces were prepared by electrochemical etching and subsequent oxidation [16, 17]. The activation with cobalt sulfide was performed by applying the routine described above. Figure 10 shows typical SEM images for a successful direct Ni metallization of an oxidized porous n-Si surface using this approach. Similarly as on polymer substrates, the metallization occurs by a fast lateral propagation of the Ni layer, which covers perfectly the surface profile.

Conclusions

The etching of polymer surfaces in chromic acid increases the surface energy due to both the increase of

References

1. Sacher E, Piraeux JJ, Kovalczyck SP (1990) Metallization of polymers. American Chemical Society, Washington
2. Hupe J, Kronenberg W (Blasberg Oberflächentechnik) (1989) Pat Appl, PCT/EP89/00204
3. Schattka D, Winkels S, Schultze JW (1997) Metalloberfläche 5:1823
4. Pilyte S, Valiuliene G, Zieliene A, Vinkevicius J (1997) J Electroanal Chem 436:127
5. Vinkevicius J, Mozginskie I, Jasulaitiene V (1998) J Electroanal Chem 442:73
6. Vaskelis A, Norkus B, Rozovskis G, Vinkevicius J (1997) Trans IMF 75:1
7. Möbius A, Pies P, Könighofen A (2000) Metalloberfläche 54:3
8. Möbius A (2000) J Oberflächetechnik 14
9. Möbius A, et al. (Enthone OMI) (2000) Pat Appl, PCT/US99/26066
10. Chan H (1992) Polymer surface modification and characterization. Hanser, Munich
11. Brocherieux A, Dessaux O, Goumand P, Gengembre L, Grimblot J, Brunel M, Razzaroni R (1995) Appl Surf Sci 90:47
12. Ha SW, Hauert R, Ernst KH, Wintermantel E (1997) Surf Coat Technol 96:293
13. Veeramasuneni S, Drelich J, Miller JD, Yamauchi G (1997) Prog Org Coat 31:265
14. Packham DE (1996) Int J Adhesion Adhesives 16:121
15. Duca M, Plosceanu C, Pop T (1998) Polymer Degrad Stab 61:65
16. Zhang XG (2001) Electrochemistry of silicon and its oxide. Kluwer, New York
17. Lehmann V (2002) Electrochemistry of silicon: instrumentation, science, materials and applications. Wiley-VCH, Weinheim